Gelation of plasmonic metal oxide nanocrystals by polymer induced depletion attractions

Camila A. Saez Cabezas[a], Gary K. Ong[a,b], Ryan B. Jadrich[a], Beth A. Lindquist[a], Ankit Agrawal[a], Thomas M. Truskett[a,c,1], and Delia J. Milliron[a,1]

[a]McKetta Department of Chemical Engineering, The University of Texas at Austin, Austin, TX 78712; [b]Department of Materials Science and Engineering, University of California, Berkeley, CA 94720; and [c]Department of Physics, The University of Texas at Austin, Austin, TX 78712

Edited by Catherine J. Murphy, University of Illinois at Urbana–Champaign, Urbana, IL, and approved July 26, 2018 received for review April 22, 2018)

Gelation of colloidal nanocrystals emerged as a strategy to preserve inherent nanoscale properties in multiscale architectures. However, available gelation methods to directly form self-supported nanocrystal networks struggle to reliably control nanoscale optical phenomena such as photoluminescence and localized surface plasmon resonance LSPR) across nanocrystal systems due to processing variabilities. Here, we report on an alternative gelation method based on physical internanocrystal interactions: short-range depletion attractions balanced by long-range electrostatic repulsions. The latter are established by removing the native organic ligands that passivate tin-doped indium oxide ITO) nanocrystals while the former are introduced by mixing with small PEG chains. As we incorporate increasing concentrations of PEG, we observe a reentrant phase behavior featuring two favorable gelation windows; the first arises from bridging effects while the second is attributed to depletion attractions according to phase behavior predicted by our unified theoretical model. Our assembled nanocrystals remain discrete within the gel network, based on X-ray scattering and high-resolution transmission electron microscopy. The infrared optical response of the gels is reflective of both the nanocrystal building blocks and the network architecture, being characteristic of ITO nanocrystals LSPR with coupling interactions between neighboring nanocrystals.

colloidal gel assembly reentrant phase behavior small-angle X-ray scattering plasmon

Nanocrystals, owing to their unique and highly tunable optical properties (1–5), hold promise as key constituents in next-generation optoelectronic materials and devices (1, 6–10). Rich opportunities to enhance and diversify materials functionality motivate the development of multiscale nanocrystal architectures via bottom-up approaches (11) because the collective properties of nanocrystals in assemblies depend on their organization. Nanoscale optical phenomena such as photoluminescence and localized surface plasmon resonance (LSPR) are especially responsive to electronic and electromagnetic coupling arising between nanocrystals in close proximity. This effect is reflected in the optical properties of extended and dense nanocrystal assemblies with a high degree of internanocrystal connectivity [e.g., superlattices (12, 13) and films (14)], which deviate from those of their isolated components. Nanocrystal gels, where nanocrystal building blocks are directly assembled into solid-like networks (i.e., a scaffold is not needed to form a stable gel), provide a unique framework to explore such structure–property relationships by allowing control over nanocrystal volume fraction, nanocrystal valence (15–17), and network topology [shape (18), size (18, 19), and density (20) of aggregates] in ways not typical of higher-density and ordered assemblies. Nanocrystal gels potential to exhibit properties both dependent on their self-assembled architecture and reflective of their nanosized building blocks has been realized for semiconductor quantum dot gels and aerogels (21), which exhibit excitonic photoluminescence that is red-shifted from the luminescence of isolated quantum dots due to energy migration through the gel network. However, plasmonic metal nanoparticles such as gold or silver fuse into wire-like networks when assembled into self-supported nanoparticle gels, obliterating the LSPR optical response characteristic of the isolated nanoparticles (22, 23). We sought a new strategy for gelation using physical bonding interactions, which we hypothesized could maintain the discrete morphology of LSPR-active metal oxides intact, to target LSPR-active nanocrystal gels. Our approach is not specific to the chemistry of the nanocrystals employed and could potentially enable a broad class of gels assembled from diverse nanoscale components capable of reflecting their individual properties.

Gelation of colloidally stable nanocrystal dispersions is achieved by balancing attractions and repulsions. In previously published examples, these interactions are simultaneously tuned by progressive oxidative ligand removal or controlled chemical bridging between surface bound species and linking agents (e.g., ions or molecules). The former has been adapted across noble metal (22, 24–27), metal chalcogenide (20, 28–31), and metal oxide (32–36) systems, but this method is prone to fuse nanocrystals (i.e., eliminate interparticle spacing) as their exposed surfaces come in contact due to a lack of stabilization, which consequently limits the realization of size- and shape-dependent optical properties (i.e., photoluminescence and LSPR) within nanocrystal gels. While gelation via chemical bridging is a viable strategy to mitigate nanocrystal fusing, translating this approach across nanocrystal materials requires customizing surface functional groups for specific nanocrystal compositions, so far limited to metal chalcogenide nanocrystals (37, 38) and gold

Significance

Self-supported gelation of optically active nanocrystals offers a modular pathway to harness optoelectronic functionality in multiscale materials by directly controlling volume fraction, bonding, and structure during assembly. We combine depletion attractions that emerge from the incorporation of small polymer chains and electrostatic repulsions to induce the gelation of isotropic metal oxide nanocrystals. We develop a theoretical model to assess our experimental fluid-to-gel-phase progression observations. By preventing nanocrystal fusion during network assembly, we achieve gels with a strong near-infrared absorption, reminiscent of the inherent near-infrared localized surface plasmon resonance of the nanocrystal building blocks.

Author contributions: C.A.S.C., G.K.O., R.B.J., B.A.L., A.A., T.M.T., and D.J.M. designed research; C.A.S.C., G.K.O., R.B.J., B.A.L., and A.A. performed research; C.A.S.C., G.K.O., R.B.J., B.A.L., A.A., T.M.T., and D.J.M. analyzed data; and C.A.S.C., G.K.O., R.B.J., B.A.L., A.A., T.M.T., and D.J.M. wrote the paper.

The authors declare no conflict of interest.

This article is a PNAS Direct Submission.

[1]To whom correspondence may be addressed. Email: truskett@che.utexas.edu or milliron@che.utexas.edu.

This article contains supporting information online at www.pnas.org/lookup/suppl/doi:10.1073/pnas.1806927115/-/DCSupplemental.

Published online August 20, 2018.

nanoparticles (23). However, even this approach did not prevent fusing of gold nanoparticles into nanowires with a concomitant loss of LSPR response. Among the sparse reports on metal oxide nanocrystal gels, gelation has been most often achieved by fusion upon ligand removal (34–36) or by triggering the entanglement of concentrated anisotropic nanoparticles: titania chains generated by oriented attachment of destabilized nanocrystals (33, 39–41) form gels upon heating, while tungsten oxide nanowires (42) and yttria nanosheets (43) form gels upon centrifugation. Once more, this approach offers limited control over gel structure and thereby the associated properties, and it cannot be easily generalized to assemble discrete isotropic metal oxide nanocrystals.

In light of these limitations, we were motivated to develop an alternative route for nanocrystal gelation based upon nonspecific physical interactions by combining depletion attractions and electrostatic repulsions. Previous studies have demonstrated that this combination can help drive the gelation of polymer colloids (44–46) and the assembly of proteins [into gels (47), clusters (48), and crystals (49, 50)], and hence it holds potential for tunable gelation of nanocrystals. Conceptual understanding of the strength and the range of depletion attractions requires consideration of only a few parameters: the concentrations of the primary colloid and the depletant (smaller, weakly interacting cosolute) and their relative dimensions. The addition of long-range repulsions to depletion interactions can favor "open" gel structures as opposed to dense colloidal phases (15, 18, 51). Therefore, a method to controllably introduce repulsive forces, here electrostatics, is needed to realize nanocrystal gelation via physical depletion attractions.

In this study, we demonstrate PEG-mediated gelation of tin-doped indium oxide (ITO) nanocrystals stripped of their native ligand shell. The ligand removal procedure employed here prevents ITO fusion into wire-like morphologies, in part by promoting electrostatic stabilization of nanocrystals as a colloid. Accordingly, bare ITO nanocrystal surfaces enable long-range repulsions, while introducing short-chain PEG triggers depletion attractions. We investigate the influence of PEG concentration ([PEG]) on competing internanocrystal interactions for a fixed nanocrystal volume fraction, and we observe two gelation thresholds at distinct [PEG], each preceded by a fluid regime (i.e., flowing dispersion) of discrete nanocrystal clusters. Since PEG is known to adsorb onto acidic metal oxide surfaces, we attribute the emergence of a first gelation window at low [PEG] to bridging of neighboring ITO nanocrystals by PEG chains, while the higher [PEG] gelation window is attributed to depletion attractions. To support our assertion and assess the gelation mechanism, we compare our experimental results to thermodynamic phase behavior predictions from a unified theory formulated to capture polymer-mediated bridging and depletion attractions. Our gelation approach effectively achieves optically active and transparent gels with LSPR similar to that of discrete ITO nanocrystals, but shifted and broadened by internanocrystal coupling. To explore the influence of network topology on optical properties, we perform far-field and near-field electromagnetic simulations based on structural information extracted from small-angle X-ray scattering (SAXS). Our simulation results predict near-field enhancement manifested as "hot spots" within the gel network that may be leveraged in future studies for energetic coupling between LSPR and molecular vibrational modes (52), or other optical transitions (53).

Results and Discussion

Our nanocrystal gelation strategy leverages physical bonds formed by balancing long-range electrostatic repulsions due to surface charge and short-range attractions induced by depletants, aiming to create stable open, arrested, and percolated networks. Charge-stabilized nanocrystals in acetonitrile with an average radius R_{ITO} of 2.83 ± 0.36 nm (*SI ppendix*, Fig. S1) were selected as the primary colloid and the source of electrostatic repulsions (see *SI ppendix*, section S2 and Figs. S2 and S3 for synthetic details). Short PEG polymer chains (number average molar mass = 1,100 g/mol) were selected as depletants based on the following criteria: the need for a cosolute with a radius of gyration, $R_{g\ PEG}$, smaller than R_{ITO}, PEG s ability to raise the osmotic pressure in solutions (54), and PEG s compatibility with polar aprotic solvents (*SI ppendix*, Fig. S4). We estimated $R_{g\ PEG}$ of these PEG chains in acetonitrile to be 0.98 nm from SAXS sizing analysis (*SI ppendix*, Fig. S5), which is in good agreement with the expected $R_{g\ PEG}$ from literature (55), to ensure that the depletant size criterion would be fulfilled. Previous studies on polymer-induced depletion attractions have shown that the strength of the attraction is tunably increased as a function of depletant concentration, which in turn dictates the extent of the network s connectivity (18, 45), affecting gel structure and any properties dependent on the local environment and valence of nanocrystals in the network. Since colloidal nanocrystal depletion gels have not been previously reported, the conditions to induce gelation were discovered by varying the amount of PEG in a charge-stabilized nanocrystal dispersions of fixed volume fraction (see *Methods* and *SI ppendix*, section S2 for additional assembly details). Experimentally, as we progressively increase the PEG concentration at a fixed nanocrystal volume fraction (4.00 vol ; *SI ppendix*, Table S1), we observe a fluid (i.e., flowing dispersion) up to a first threshold for gelation at [PEG] = 46.0 mM, then reentrant behavior back to a flowing dispersion, followed by a second occurrence of a gel at [PEG] = 534 mM (Fig. 1, *Insets*).

To investigate the conditions that enabled gelation and to characterize the fluid regime, the ITO–PEG mixtures formed at different [PEG] were probed with SAXS. Specifically, we examine the structure factor S(q) as a function of [PEG] by removing the form factor contribution to the SAXS data (see *SI ppendix*, section S1 for more details and *SI ppendix*, Fig. S6) to gain insight into the physical origins of the self-assembly. As a result, we identify two distinct interaction regimes (Fig. 1). First, we note a prominent S(q) peak (q ~ 0.023 Å^{-1}; Fig. 1) for the ITO–PEG flowing dispersion of lowest [PEG] emerging at a lower q than that indicative of correlations between directly

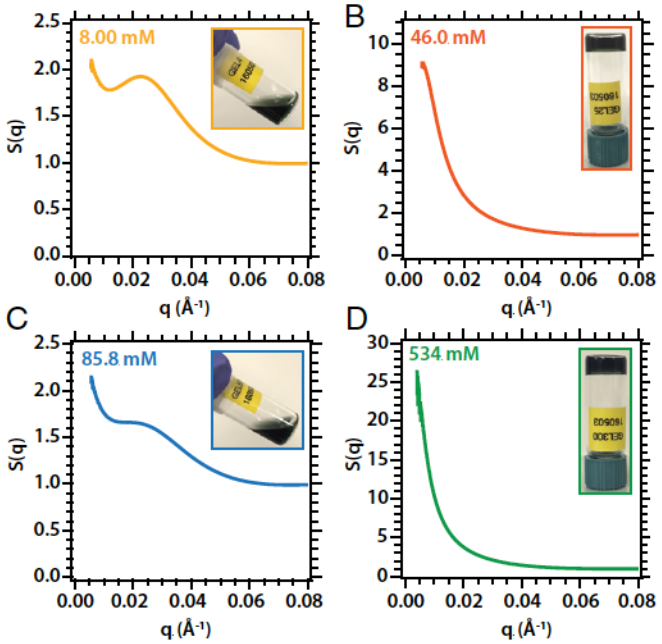

Fig. 1. SAXS characterization of the ITO–PEG flowing dispersions and gels. *A*) Structure factor S q) of flowing dispersion with [PEG] = 8.00 mM, *B*) S q) of gel with [PEG] = 46.0 mM, *C*) S q) of flowing dispersion with [PEG] = 85.8 mM, and *D*) S q) of gel with [PEG] = 534 mM. S q) plots are accompanied with photograph insets of the corresponding ITO–PEG mixture.

adjacent nanocrystals [see *SI Appendix*, Fig. S7 for full q range S(q)], thus characteristic of intermediate range order in colloidal assemblies (51, 56, 57). Considering the intermediate range order behavior of this ITO–PEG mixture ([PEG] = 8.00 mM), we establish that competing short-range attractions and long-range repulsions frustrate large-scale aggregation and lead to the formation of discrete nanocrystal clusters (~270-Å length scale). In addition, we observe similar intermediate range order behavior for the flowing dispersions in the reentrant regime (Fig. 1*C* and *SI Appendix*, Fig. S8). Although the S(q) peaks near $q \sim 0.02$ Å^{-1} are less pronounced and broadened, likely due to an increase in attraction strength and cluster polydispersity, the presence of dispersed discrete clusters is still apparent in the reentrant regime. Second, in all cases, we observe that S(q) diverges as q approaches zero, suggesting systems dominated by attractions and thermodynamic compressibility (51, 56). In particular, the S(q) intensity at the lowest resolvable q is approximately an order of magnitude higher when gelation occurs compared with the S(q) intensity of all flowing cluster dispersions (Fig. 1 *B* and *D*). Prior colloidal assembly studies (15, 58–60) have reported a comparable S(q) intensity increase (of an order of magnitude or larger) when a colloidal system transitions from a fluid state to a gel through spinodal decomposition.

Further inspection of S(q) for both low and high [PEG] gels by employing Beaucage s unified function (61–63) approach for complex structures provides insight into the structural hierarchy of the gels and their respective fractal dimension (D_f). First, the number of apparent structural length scales along with their respective limits are determined from a derivative analysis (*SI Appendix*, Fig. S9). Following this method, we identify two distinct structural length scales in the S(q) of the high [PEG] gel, whereas the S(q) of the low [PEG] gel only exhibits one. Thereafter, our derivative analysis results guide the S(q) unified fitting of both gels (*SI Appendix*, Fig. S10). While the S(q) of the [PEG] = 46.0 mM gel scatters as a mass fractal of $D_f = 2.2$, the S(q) of the [PEG] = 534 mM gel is composed of a mid-q (0.04 Å$^{-1} < q < 0.058$ Å^{-1}) scattering contribution from nanocrystal clusters plus a low-q (0.01 Å$^{-1} < q < 0.02$ Å^{-1}) scattering contribution attributed to the presence of a percolated fractal gel network ($D_f = 2.09$). For both low and high [PEG], we associate gelation with slow bonding kinetics since the fitted D_f values fall within the expected range (2.0–2.2) for reaction-limited cluster aggregation systems (64–66).

In the SAXS data of all [PEG] we observe the form factor of the discrete nanocrystal spheres, with fitting results yielding constituent particles with a radius of 2.95, 2.89, and 2.82 nm in the case of the lowest [PEG] dispersion, low-[PEG] gel, and high-[PEG] gel, respectively. This consistency suggests that the nanocrystals remain discrete under all PEG-induced assembly conditions. The persistence of the nanocrystals morphology is further supported by high-resolution transmission electron microscopy imaging of a dried and diluted gel with [PEG] = 534 mM (*SI Appendix*, Fig. S11), where individual nanocrystals are discerned without apparent crystallographic continuity (i.e., oriented attachment) between them. Detecting a prevalent crystallographic orientation continuous between neighboring nanocrystals would suggest internanocrystal fusion since metal oxides are known to fuse into extended nanostructures by oriented attachment (67, 68). Scherrer analysis of X-ray diffraction complements our observations by high-resolution transmission electron microscopy, where the crystallite size of discrete ligand-stripped nanocrystals [6.19 nm for the (222) peak] is found to be comparable to the nanocrystal size in the gel with [PEG] = 534 mM [5.89 nm for the (222) peak; see *SI Appendix*, Fig. S12], both of which are in turn consistent with diameters measured by electron microscopy, SAXS, and dynamic light scattering. Preventing nanocrystal fusion throughout the assembly process is particularly advantageous for depletion gelation since the attraction strength can be weakened by reducing the depletant concentration relative to the primary particle and, in principle, reverse gelation. We achieved the disassembly of the ITO–PEG gel ([PEG] = 534 mM) by adding 600 L of ITO–PEG flowing dispersion ([PEG] = 8.00 mM) to dilute [PEG] in the mixture by a factor of three at a fixed nanocrystal vol (Movie S1). A stable flowing dispersion is recovered by gentle manual agitation without using sonication or vortexing.

Considering the [PEG]-dependent phase progression including a reentrant regime, we hypothesized that gelation might be influenced by internanocrystal attractions other than depletion attractions. Specifically, we propose that, in addition to its depletant role, PEG can bridge adjacent ITO nanocrystals. Because PEG chains are known to preferentially adsorb on acidic oxide surfaces (the isoelectric point of the nanocrystals used in this work is between 4 and 5; *SI Appendix*, Fig. S13) via hydrogen bonding and subsequently aggregate oxide particles (69–71), we deduce that low PEG concentrations (e.g., [PEG] = 46.0 mM) can favor bridging gelation. It is worth noting that PEG adsorption on the metal oxide surface does not hinder the internanocrystal long-range electrostatic repulsion necessary to form open depletion gels since dispersed ITO–PEG clusters still exhibit a strong positive zeta potential (*SI Appendix*, Fig. S14). In this light, prior work by Luo et al. (45) and Zhao et al. (72) described an analogous experimental phase progression in a polystyrene microsphere system where bridging and depletant effects are both operative. They showed the emergence of the following phase transition sequence as the concentration of the smaller adsorbing species [poly(*N*-isopropylacrylamide)] in the system increases: bridging-induced aggregation stabilization of discrete microspheres depletion-induced aggregation. Moreover, they determined that since depletion-attraction interactions are only favored once the adsorbing molecules have saturated the colloidal surface and bridging attractions are hindered, the assembly mechanism (i.e., bridging or depletion) is highly sensitive to changes in the colloid-to-adsorbing molecule concentration ratios.

To assess our proposed mechanism for reentrant gelation in ITO–PEG dispersions, we devised a theoretical model that is unique in possessing a unified description of bridging and depletion effects. The free-energy theory synergistically combines a well-accepted theoretical treatment for the Asakura Oosawa model (depletion) with the accurate Wertheim theory for strong association (bridging). As detailed microstructural prediction is not our goal, simplification comes from approximating the stabilizing repulsions with hard-core interactions for the purposes of bulk thermodynamic calculations (73, 74). Various physical parameters enter the theory: the nanocrystal-to-polymer diameter ratio (d_{NC}/d_P), the number of polymers that can adsorb onto the nanocrystal surface before saturation (n_{ads}), the number of nanocrystals that a single polymer chain can bridge (n_{bind}), and the polymer-nanocrystal thermal adsorption volume (v), which encapsulates the combined effects of adsorption energy, temperature, and the spatial range of the attraction (see *Methods* and *SI Appendix* for more details). To specifically model our nanocrystal gels, for d_{NC}/d_P we use the experimental value of ~3, and for n_{bind} we use the physically reasonable value of 2 based on the short PEG chains employed and nanocrystal size. For v and n_{ads} we explored various possibilities and the associated phase behavior, one example of which is shown in Fig. 2 for $n_{ads} = 30$ and $v = 0.181$ yielding a reentrant (liquid gel liquid gel) phase diagram that is almost quantitatively in accord with the experimental results. Given our choices above for n_{ads} and n_{bind}, zero-temperature mean-field theoretical calculations (16) indicate that the bridging regime should not exceed a polymer-to-colloid ratio of 435 at any volume fraction or value of v. Therefore, the first spinodally unstable regime with increasing depletant is driven by nanocrystal–polymer bridging (which saturates upon surface coating) and the second by depletion. Importantly, the phase diagram is always qualitatively the same for physically reasonable values of n_{ads}: bridging gels form when the ratio of the number of polymers per nanocrystal is of the order of 10–100, whereas of the order of 1,000 is required for depletion—as seen in the experiments.

Our nanocrystal gels assembled via bridging and depletion interactions are optically active and exhibit an extinction

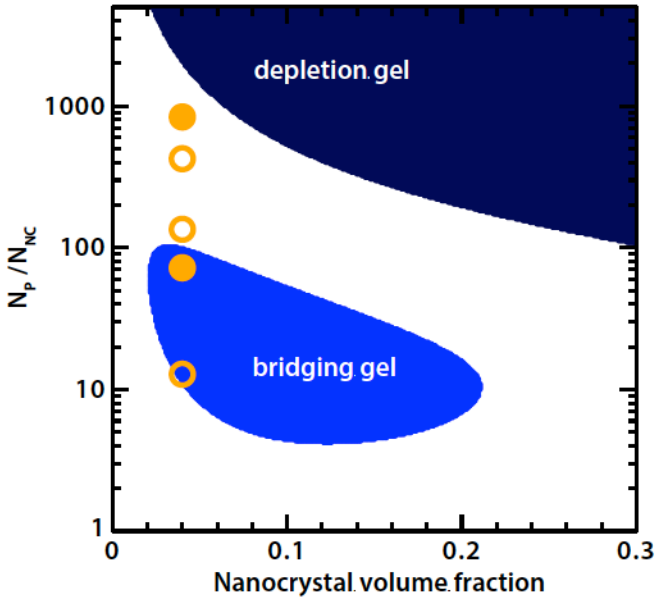

Fig. 2. Comparison of theoretical model to experimental observations. Theoretical phase diagram overlaid with experimental data points. N_p/N_{NC} denotes the ratio of number of polymers per nanocrystal. Open circles represent experimental flowing dispersions and closed circles represent experimental observation of gels. Regions where bridging and depletion gelation are predicted to occur are delimited by light- and dark-blue areas, respectively.

spectrum reminiscent of that of the discrete nanocrystal building blocks. As shown in Fig. 3 , the LSPR peak of both the bridging ([PEG] = 46.0 mM) and depletion ([PEG] = 534 mM) gels is red-shifted (by 212 and 101 cm ^{1} for the bridging and depletion gel, respectively) from that of dispersed nanocrystals in acetonitrile. We attribute the similarity between these spectra to our successful preservation of the nanocrystal morphology as they are integrated in the gel network, avoiding ITO nanocrystal fusion by oriented attachment (*SI ppendix*, Figs. S11 and S12). The modest red shift of both gel LSPRs, their reduced peak intensity, and significant broadening toward lower energies compared with the spectrum of isolated nanocrystals are all characteristic of LSPR coupling between nearest neighbors, as previously studied in extended assemblies, such as films of colloidal metal nanoparticles (75–77) and metal oxide nanocrystals (52, 78, 79). Moreover, considering our gel structure analysis from SAXS, we hypothesized that the difference in LSPR peak broadening and shifting between the bridging and depletion gels is correlated to their structural differences. Since the depletion gel network is composed of discrete nanocrystal clusters, not detected in the bridging gel network, we expect the gel LSPR to be affected by variations in the nearest-neighbor environment of nanocrystals.

To investigate the influence of nanocrystal clustering on the gel s far-field optical properties and to anticipate near-field optical properties, we simulated the optical response of an extended network composed of PEG-coated ITO octahedral clusters (10 nm in radius) with a nanocrystal volume fraction of 3.88 vol , similar to that of the depletion gel studied experimentally (see *SI ppendix* for more details). Although an idealized structural representation was used to ensure computational tractability, the simulated network was designed to approximate the experimentally measured nanocrystal volume fraction in the gel and the structural hierarchy ascertained from analysis of the SAXS data described earlier. As shown in Fig. 3*B*, the simulated depletion gel LSPR does not precisely capture the features of the experimental depletion gel LSPR due to simulation limitations, mainly the size of the simulated box. Nonetheless, the simulated spectrum qualitatively reflects the LSPR characteristics of the bridging and depletion configurations, thus highlighting the optical sensitivity to LSPR–LSPR coupling facilitated by arranging ITO nanocrystal building blocks in close proximity in the gel network. Based on the simulations, we anticipated that such coupling effects should give rise to intense "hot spots" of greatly enhanced electric field intensity confined between nanocrystals in gel assemblies where the electromagnetic near-fields of neighboring constituents overlap. Simulated near-field maps shown in Fig. 3*C* demonstrate the near-field enhancement under resonant optical excitation of the ITO nanocrystal gel network.

Altogether, these findings support nanocrystal gel assemblies potential to achieve highly tunable and complex plasmonic materials by leveraging the dependence of optical properties on the mesoscale arrangement of discrete nanocrystal building blocks. In addition, assembling closely spaced nanocrystals into a gel network allows generation of localized hot spots, thereby providing coupling opportunities to other optical transitions relevant to surface enhanced infrared absorption spectroscopy and sensing applications (10, 52, 80) otherwise inaccessible in networks built from crystallographic junctions of fused nanocrystals.

Conclusion and Outlook

The strategy described here demonstrates the potential for tunable gels based on reversible physical bonds, and with responsive optical properties. A basic requirement for optical materials is that scattering does not interfere with the absorption, reflection, and luminescence properties of interest. Our depletion-attraction strategy produces a highly transparent ITO nanocrystal gel that remains stable for over 1 year without developing haze noticeable to the eye (Fig. 3*D*). Obtaining transparent self-supported nanocrystal gels has remained a challenge in the field since most established gelation methods give rise to fast-growing networks of large aggregates (scatterers) that ultimately form opaque gels. Instead, as alluded to earlier for our system, competing electrostatic repulsions and attractions (via bridging or depletion) favor slow bonding kinetics and thereby facilitate the formation of fractal aggregates with characteristic length scales smaller than the wavelength of visible light (R_g = 13.6 and 53.0 nm for bridging and depletion gel, respectively; *SI ppendix*, Fig. S10). Our results are consistent with a previous study by Korala and Brock (19) on the aggregation kinetics of CdSe in which it was determined that

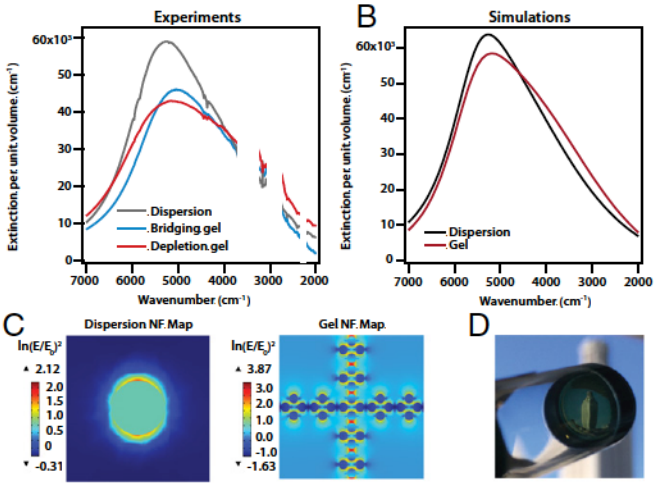

Fig. 3. Experimental and simulated optical properties of ITO–PEG gels. *A*) Experimental extinction spectra of depletion gel [PEG] = 534 mM, red), bridging gel [PEG] = 46.0 mM, blue), and ligand-stripped nanocrystal dispersion gray), *B*) simulated extinction spectra of nanocrystal gel and ligand-stripped nanocrystal dispersion, *C*) simulated near-field NF) maps of nanocrystal gel and ligand-stripped nanocrystal dispersion, and *D*) photograph of highly transparent nanocrystal depletion gel under natural lighting against the University of Texas Tower.

simultaneously accessing the reaction-limited clustering aggregation regime and suppressing large-scale aggregation are necessary conditions to induce transparency in a nanocrystal gel. Accordingly, gaining insight into the interplay between interparticle interactions, structure, and aggregation kinetics is key to rationalize and exploit the nanocrystal gel properties stemming from nanoscale building blocks.

More generally, we showed how the combination of depletion attractions and electrostatic repulsions can realize the assembly of nanocrystal gels. While the addition of PEG mediates attractions between dispersed nanocrystals, competing long-range electrostatic repulsions resulting from ligand stripping encourage the formation of a self-supported gel rather than a dense and collapsed material. We observed the emergence of two gelation windows interspaced with flowing dispersion states of discrete nanocrystal clusters. Transitioning from a flowing to a solid-like gel state was accompanied by a strong S(q) divergence and intensity increase at the lowest resolvable q, a characteristic of colloidal aggregation through spinodal decomposition reported in prior literature. In this regard, our theoretical phase behavior predictions, based on a unified bridging and depletion-attraction description that captured PEG s affinity for oxide surfaces and ability to bridge adjacent ITO nanocrystals, supported our experimental results and identified two spinodally unstable regions favoring bridging and depletion gelation at low and high [PEG], respectively. Moreover, we structurally differentiated the dominant assembly mechanism in each gel by recognizing two scattering length scales (nanocrystal < fractal gel) in the bridging gel as opposed to the three scattering length scales (nanocrystal < cluster < fractal gel) apparent in the depletion gel likely due to depletion attractions acting on preassembled clusters instead of discrete nanocrystals.

Our ITO nanocrystal model system was selected to investigate the gelation of charge-stabilized nanocrystals driven by depletion attractions, to experimentally demonstrate its feasibility, and to develop an adaptable gelation strategy that should in principle be broadly applicable across nanocrystal systems. For instance, other nanocrystal compositions with size and zeta potential similar to our nanocrystals are already available by established colloidal syntheses and represent the most immediate candidates to extend this work. Based on our analysis, depletant molecular weight may be varied to achieve similar assembly results with nanocrystals of different sizes. Also, as long as internanocrystal electrostatic repulsions are sufficient for colloidal stabilization, similar phase behavior is expected. Since bridging attractions between nanocrystals and depletants depend on surface chemical interactions, nanocrystal and depletant compositions can be strategically paired to tune bridging gelation or even suppress its emergence.

From an application perspective, we demonstrated optically active nanocrystal gels featuring LSPR representative of the nanocrystal building blocks by retaining their discrete morphology in the network, which has not been achieved with previously reported self-supported gel processing methods for plasmonic nanoparticles. By limiting the extent of aggregation, our gelation approach favored the formation of transparent gels, showing no signs of visible haze or scattering. In addition, we compared our optical spectra from experiments to electromagnetic simulations to highlight near-field enhancement opportunities generated by nearest-neighbor coupling effects in the gel network, a promising feature that encourages further exploring nanocrystal gels as an alternative material for coupling applications. Finally, we envision that extending our gelation approach to other nanocrystal systems could motivate further studies to improve our insight on structure–property relationships in assemblies to thus achieve systematic design of nanocrystal gel properties. We believe that our framework could also contribute to the development and diversification of multicomponent nanocrystal gels as a means to unlock even more complex nanocrystal gel functionality.

Methods

ITO PEG Assemblies ITO nanocrystals were synthesized using established colloidal synthesis methods and ligand-stripped by a postsynthetic chemical treatment. Ligand-stripped nanocrystals dispersed in a PEG–acetonitrile solution were combined with incremental amounts of PEG to form flowing dispersions and gels. The samples were kept in sealed vials and remained unperturbed during the self-assembly process. Additional synthetic, ligand-stripping, and assembly details are described in *SI Appendix*, section S2.

SAXS Characterization SAXS measurements were performed at the Lawrence Berkeley National Laboratory Advance Light Source beamline 7.3.3 at 3.8-m sample–detector distance. All ITO–PEG samples were enclosed in flame-sealed glass capillaries and measured in transmission configuration *SI Appendix*, section S2).

Unified Theoretical Bridging and Depletion Gelation Model Phase diagram predictions utilize an approximate free energy expression for the Asakura Oosawa model modified to include short-range polymer–nanocrystal surface attractions. Formally, the free energy is decomposed as $a \equiv a_{AO}$ $a_B^{(ex}$, where a_{AO} and $a_B^{(ex}$ are the Asakura Oosawa and excess bonding from polymer–nanocrystal adsorption) free energy contributions. For a_{AO} we employ the theory of Lekkerkerker et al. 81) and for $a_B^{(ex}$ we use Werthiem first-order association theory 82, 83). Spinodal boundaries are identified from the Hessian matrix) of partial derivatives with respect to polymer and nanocrystal densities by the satisfaction of det ≤ 0. For more details, see *SI Appendix*, section S3.

LSPR Measurement and Analysis UV-visible and infrared spectroscopy techniques were used to collect absorption spectra. Samples were enclosed in a liquid cell with calcium fluoride windows. To calculate extinction cross-sections, the Beer–Lamberts law was used. To simulate the optical property of the ITO–PEG gels, an idealized PEG-coated ITO nanocrystal network was designed using the design module in COMSOL. For more details, see *SI Appendix*, sections S2 and S4.

ACKNOWLEDGMENTS. We thank Angela M. Wagner for her assistance with isoelectric point measurement and Corey M. Staller for his assistance with inductively coupled plasma spectroscopy. This work was primarily supported by the NSF through the Center for Dynamics and Control of Materials: an NSF Materials Research Science and Engineering Center MRSEC) under Cooperative Agreement DMR-1720595. SAXS data were collected at the Advanced Light Source s beamline 7.3.3 at the Lawrence Berkeley National Laboratory, a user facility supported by the US Department of Energy Office of Science under Contract DE-AC02CH11231. This work was also supported by NSF Graduate Research Fellowship DGE-1106400 to G.K.O.), Welch Foundation Grants F-1848 and F-1696, and NSF Grants CHE-1609656 and CBET-1247945.

1. Talapin DV, Lee J-S, Kovalenko MV, Shevchenko EV 2010) Prospects of colloidal nanocrystals for electronic and optoelectronic applications. *Chem Rev* 110: 389–458.
2. Giannini V, Fernández-Domínguez AI, Heck SC, Maier SA 2011) Plasmonic nanoantennas: Fundamentals and their use in controlling the radiative properties of nanoemitters. *Chem Rev* 111:3888–3912.
3. Agrawal A, Johns RW, Milliron DJ 2017) Control of localized surface plasmon resonances in metal oxide nanocrystals. *Annu Rev Mater Res* 47:1–31.
4. Pu C, et al. 2017) Synthetic control of exciton behavior in colloidal quantum dots. *J Am Chem Soc* 139:3302–3311.
5. Agrawal A, et al. 2018) Localized surface plasmon resonance in semiconductor nanocrystals. *Chem Rev* 118:3121–3207.
6. Runnerstrom EL, Llordés A, Lounis SD, Milliron DJ 2014) Nanostructured electrochromic smart windows: Traditional materials and NIR-selective plasmonic nanocrystals. *Chem Commun Camb)* 50:10555–10572.
7. Carey GH, et al. 2015) Colloidal quantum dot solar cells. *Chem Rev* 115: 12732–12763.
8. Pietryga JM, et al. 2016) Spectroscopic and device aspects of nanocrystal quantum dots. *Chem Rev* 116:10513–10622.
9. Wang Y, Runnerstrom EL, Milliron DJ 2016) Switchable materials for smart windows. *Annu Rev Chem Biomol Eng* 7:283–304.
10. Jiang N, Zhuo X, Wang J 2018) Active plasmonics: Principles, structures, and applications. *Chem Rev* 118:3054–3099.
11. Boles MA, Engel M, Talapin DV 2016) Self-assembly of colloidal nanocrystals: From intricate structures to functional materials. *Chem Rev* 116:11220–11289.
12. Murray CB, Kagan CR, Bawendi MG 2000) Synthesis and characterization of monodisperse nanocrystals and close-packed nanocrystal assemblies. *Annu Rev Mater Sci* 30:545–610.
13. Chen C-F, Tzeng S-D, Chen H-Y, Lin K-J, Gwo S 2008) Tunable plasmonic response from alkanethiolate-stabilized gold nanoparticle superlattices: Evidence of near-field coupling. *J Am Chem Soc* 130:824–826.

14. Wang H, Levin CS, Halas NJ 2005) Nanosphere arrays with controlled sub-10-nm gaps as surface-enhanced Raman spectroscopy substrates. *J Am Chem Soc* 127: 14992–14993.
15. Zaccarelli E, Lu PJ, Ciulla F, Weitz DA, Sciortino F 2008) Gelation as arrested phase separation in short-ranged attractive colloid–polymer mixtures. *J Phys Condens Matter* 20:494242.
16. Lindquist BA, Jadrich RB, Milliron DJ, Truskett TM 2016) On the formation of equilibrium gels via a macroscopic bond limitation. *J Chem Phys* 145:074906.
17. Ruzicka B, et al. 2011) Observation of empty liquids and equilibrium gels in a colloidal clay. *Nat Mater* 10:56–60.
18. Sciortino F, Tartaglia P, Zaccarelli E 2005) One-dimensional cluster growth and branching gels in colloidal systems with short-range depletion attraction and screened electrostatic repulsion. *J Phys Chem B* 109:21942–21953.
19. Korala L, Brock SL 2012) Aggregation kinetics of metal chalcogenide nanocrystals: Generation of transparent CdSe ZnS) core shell) gels. *J Phys Chem C Nanomater Interfaces* 116:17110–17117.
20. Yu H, Liu Y, Brock SL 2009) Tuning the optical band gap of quantum dot assemblies by varying network density. *ACS Nano* 3:2000–2006.
21. Ziegler C, et al. 2017) Modern inorganic aerogels. *Angew Chem Int Ed Engl* 56: 13200–13221.
22. Herrmann A-K, et al. 2014) Multimetallic aerogels by template-free self-assembly of Au, Ag, Pt, and Pd nanoparticles. *Chem Mater* 26:1074–1083.
23. Wen D, et al. 2016) Gold aerogels: Three-dimensional assembly of nanoparticles and their use as electrocatalytic interfaces. *ACS Nano* 10:2559–2567.
24. Bigall NC, et al. 2009) Hydrogels and aerogels from noble metal nanoparticles. *Angew Chem Int Ed Engl* 48:9731–9734.
25. Liu W, et al. 2015) Noble metal aerogels-synthesis, characterization, and application as electrocatalysts. *Acc Chem Res* 48:154–162.
26. Naskar S, et al. 2017) Porous aerogels from shape-controlled metal nanoparticles directly from nonpolar colloidal solution. *Chem Mater* 29:9208–9217.
27. Nahar L, Farghaly AA, Alan Esteves RJ, Arachchige IU 2017) Shape controlled synthesis of Au/Ag/Pd nanoalloys and their oxidation-induced self-assembly into electrocatalytically active aerogel monoliths. *Chem Mater* 29:7704–7715.
28. Arachchige IU, Mohanan JL, Brock SL 2005) Sol gel processing of semiconducting metal chalcogenide xerogels: Influence of dimensionality on quantum confinement effects in a nanoparticle network. *Chem Mater* 17:6644–6650.
29. Arachchige IU, Brock SL 2007) Sol-gel methods for the assembly of metal chalcogenide quantum dots. *Acc Chem Res* 40:801–809.
30. Mohanan JL, Arachchige IU, Brock SL 2005) Porous semiconductor chalcogenide aerogels. *Science* 307:397–400.
31. Kalebaila KK, Brock SL 2012) Lead selenide nanostructured aerogels and xerogels. *Z Anorg Allg Chem* 638:2598–2603.
32. Anderson ML, Morris CA, Stroud RM, Merzbacher CI, Rolison DR 1999) Colloidal gold aerogels: Preparation, properties, and characterization. *Langmuir* 15:674–681.
33. Polleux J, Pinna N, Antonietti M, Niederberger M 2004) Ligand directed assembly of preformed titania nanocrystals into highly anisotropic nanostructures. *Adv Mater* 16: 436–439.
34. Rechberger F, Heiligtag FJ, Süess MJ, Niederberger M 2014) Assembly of $BaTiO_3$ nanocrystals into macroscopic aerogel monoliths with high surface area. *Angew Chem Int Ed Engl* 53:6823–6826.
35. Rechberger F, Mercandetti C, Tervoort E, Niederberger M 2017) Colloidal nanocrystal-based $BaTiO_3$ xerogels as green bodies: Effect of drying and sintering at low temperatures on pore structure and microstructures. *Langmuir* 33:280–287.
36. Rechberger F, Tervoort E, Niederberger M 2017) Nonaqueous sol gel synthesis of $InTaO_4$ nanoparticles and their assembly into macroscopic aerogels. *J Am Ceram Soc* 100:4483–4490.
37. Lesnyak V, et al. 2011) 3D assembly of semiconductor and metal nanocrystals: Hybrid CdTe/Au structures with controlled content. *J Am Chem Soc* 133:13413–13420.
38. Sayevich V, et al. 2016) 3D assembly of all inorganic colloidal nanocrystals into gels and aerogels. *Angew Chem Int Ed Engl* 55:6334–6338.
39. Heiligtag FJ, Rossell MD, Süess MJ, Niederberger M 2011) Template-free co-assembly of preformed Au and TiO_2 nanoparticles into multicomponent 3D aerogels. *J Mater Chem* 21:16893–16899.
40. Heiligtag FJ, Kränzlin N, Süess MJ, Niederberger M 2014) Anatase-silica composite aerogels: A nanoparticle-based approach. *J Sol-Gel Sci Technol* 70:300–306.
41. Heiligtag FJ, et al. 2014) Self-assembly of metal and metal oxide nanoparticles and nanowires into a macroscopic ternary aerogel monolith with tailored photocatalytic properties. *Chem Mater* 26:5576–5584.
42. Cheng W, Rechberger F, Niederberger M 2016) From 1D to 3D–Macroscopic nanowire aerogel monoliths. *Nanoscale* 8:14074–14077.
43. Cheng W, Rechberger F, Niederberger M 2016) Three-dimensional assembly of yttrium oxide nanosheets into luminescent aerogel monoliths with outstanding adsorption properties. *ACS Nano* 10:2467–2475.
44. Bergenholtz J, Poon WCK, Fuchs M 2003) Gelation in model colloid polymer mixtures. *Langmuir* 19:4493–4503.
45. Luo J, et al. 2015) Gelation of large hard particles with short-range attraction induced by bridging of small soft microgels. *Soft Matter* 11:2494–2503.
46. Verhaegh NAM, Asnaghi D, Lekkerkerker HNW, Giglio M, Cipelletti L 1997) Transient gelation by spinodal decomposition in colloid-polymer mixtures. *Physica A* 242: 104–118.
47. de Kruif CG, Tuinier R 2001) Polysaccharide protein interactions. *Food Hydrocoll* 15: 555–563.
48. Johnston KP, et al. 2012) Concentrated dispersions of equilibrium protein nanoclusters that reversibly dissociate into active monomers. *ACS Nano* 6:1357–1369.
49. Kulkarni A, Zukoski C 2001) Depletion interactions and protein crystallization. *J Cryst Growth* 232:156–164.
50. Whitelam S 2010) Control of pathways and yields of protein crystallization through the interplay of nonspecific and specific attractions. *Phys Rev Lett* 105:088102.
51. Jadrich RB, Bollinger JA, Johnston KP, Truskett TM 2015) Origin and detection of microstructural clustering in fluids with spatial-range competitive interactions. *Phys Rev E* 91:042312.
52. Agrawal A, et al. 2017) Resonant coupling between molecular vibrations and localized surface plasmon resonance of faceted metal oxide nanocrystals. *Nano Lett* 17: 2611–2620.
53. Akselrod GM, et al. 2016) Efficient nanosecond photoluminescence from infrared PbS quantum dots coupled to plasmonic nanoantennas. *ACS Photonics* 3:1741–1746.
54. Money NP 1989) Osmotic pressure of aqueous polyethylene glycols. *Plant Physiol* 91: 766–769.
55. Devanand K, Selser JC 1991) Asymptotic behavior and long-range interactions in aqueous solutions of poly ethylene oxide). *Macromolecules* 24:5943–5947.
56. Liu Y, et al. 2011) Lysozyme protein solution with an intermediate range order structure. *J Phys Chem B* 115:7238–7247.
57. Ong GK, et al. 2015) Ordering in polymer micelle-directed assemblies of colloidal nanocrystals. *Nano Lett* 15:8240–8244.
58. Lu PJ, et al. 2008) Gelation of particles with short-range attraction. *Nature* 453: 499–503.
59. Carpineti M, Giglio M 1992) Spinodal-type dynamics in fractal aggregation of colloidal clusters. *Phys Rev Lett* 68:3327–3330.
60. Manley S, et al. 2005) Glasslike arrest in spinodal decomposition as a route to colloidal gelation. *Phys Rev Lett* 95:238302.
61. Beaucage G 1995) Approximations leading to a unified exponential/power-law approach to small-angle scattering. *J Appl Crystallogr* 28:717–728.
62. Beaucage G 1996) Small-angle scattering from polymeric mass fractals of arbitrary mass-fractal dimension. *J Appl Crystallogr* 29:134–146.
63. Beaucage G 2012) Combined small-angle scattering for characterization of hierarchically structured polymer systems over nano-to-micron meter. *Polymer Science: A Comprehensive Reference* Elsevier, Amsterdam), pp 399–409.
64. Jullien R, Kolb M 1984) Hierarchical model for chemically limited cluster-cluster aggregation. *J Phys Math Gen* 17:L639–L643.
65. Brown WD, Ball RC 1985) Computer simulation of chemically limited aggregation. *J Phys Math Gen* 18:L517–L521.
66. Lin MY, et al. 1990) Universal reaction-limited colloid aggregation. *Phys Rev A* 41: 2005–2020.
67. Zhang J, Huang F, Lin Z 2010) Progress of nanocrystalline growth kinetics based on oriented attachment. *Nanoscale* 2:18–34.
68. Niederberger M, Cölfen H 2006) Oriented attachment and mesocrystals: Non-classical crystallization mechanisms based on nanoparticle assembly. *Phys Chem Chem Phys* 8: 3271–3287.
69. Mathur S, Moudgil BM 1997) Adsorption mechanism s) of poly ethylene oxide) on oxide surfaces. *J Colloid Interface Sci* 196:92–98.
70. Lafuma F, Wong K, Cabane B 1991) Bridging of colloidal particles through adsorbed polymers. *J Colloid Interface Sci* 143:9–21.
71. Wong K, et al. 1992) Intermediate structures in equilibrium flocculation. *J Colloid Interface Sci* 153:55–72.
72. Zhao C, Yuan G, Jia D, Han CC 2012) Macrogel induced by microgel: Bridging and depletion mechanisms. *Soft Matter* 8:7036–7040.
73. Lowen H, Roux JN, Hansen JP 1991) Mapping of charge polydispersity onto size polydispersity in colloidal suspensions. *J Phys Condens Matter* 3:997–1002.
74. Gögelein C 2008) *Phase Behaviour of Proteins and Colloid-Polymer Mixtures* Forschungszentrum Jülich, Jülich, Germany).
75. Jain PK, Huang W, El-Sayed MA 2007) On the universal scaling behavior of the distance decay of plasmon coupling in metal nanoparticle pairs: A plasmon ruler equation. *Nano Lett* 7:2080–2088.
76. Lin S, Li M, Dujardin E, Girard C, Mann S 2005) One dimensional plasmon coupling by facile self assembly of gold nanoparticles into branched chain networks. *Adv Mater* 17:2553–2559.
77. Barrow SJ, Funston AM, Gómez DE, Davis TJ, Mulvaney P 2011) Surface plasmon resonances in strongly coupled gold nanosphere chains from monomer to hexamer. *Nano Lett* 11:4180–4187.
78. Agrawal A, Kriegel I, Milliron DJ 2015) Shape-dependent field enhancement and plasmon resonance of oxide nanocrystals. *J Phys Chem C* 119:6227–6238.
79. Kim J, et al. 2015) Zinc oxide based plasmonic multilayer resonator: Localized and gap surface plasmon in the infrared. *ACS Photonics* 2:1224–1230.
80. Willets KA, Van Duyne RP 2007) Localized surface plasmon resonance spectroscopy and sensing. *Annu Rev Phys Chem* 58:267–297.
81. Lekkerkerker HNW, Poon WCK, Pusey PN, Stroobants A, Warren PB 1992) Phase behaviour of colloid polymer mixtures. *Europhys Lett* 20:559–564.
82. Jackson G, Chapman WG, Gubbins KE 1988) Phase equilibria of associating fluids. *Mol Phys* 65:1–31.
83. Chapman WG, Jackson G, Gubbins KE 1988) Phase equilibria of associating fluids. *Mol Phys* 65:1057–1079.